12-10-2019

A Wideband, Circularly Polarized, Directive Antenna With a Circular Reflector

Tyler J. McPherson

Zabed Iqbal

Sungkyun Lim

IEEE Access
Multidisciplinary | Rapid Review | Open Access Journal

Received November 18, 2019, accepted December 1, 2019, date of publication December 10, 2019,
date of current version December 23, 2019.

Digital Object Identifier 10.1109/ACCESS.2019.2958528

A Wideband, Circularly Polarized, Directive Antenna With a Circular Reflector

TYLER J. MCPHERSON[1], (Student Member, IEEE), ZABED IQBAL[2], (Student Member, IEEE), AND SUNGKYUN LIM[1], (Senior Member, IEEE)

[1]Department of Electrical and Computer Engineering, Georgia Southern University, Statesboro, GA 30460, USA
[2]Department of Electrical and Computer Engineering, The University of Alabama in Huntsville, Huntsville, AL 35899, USA

Corresponding author: Sungkyun Lim (sklim@georgiasouthern.edu)

ABSTRACT A two-element, patch antenna with a single feed is presented to achieve wideband, circular polarization, and uni-directional radiation. The driven element of the antenna has a rotated, corner-truncated radiating patch to achieve circularly polarized radiation with an offset microstrip feedline in the front side. The back side of the driven element comprises a wide hexagonal slot, eight meander tips, and a parasitic patch in the center. A circular reflector is added behind the driven element to increase realized gain toward the front side direction of the driven element. A prototype of the antenna is fabricated for validation. In both simulation and measurement, the 3-dB axial ratio bandwidth is fully included in the −10-dB impedance bandwidth. In measurement, the proposed antenna has a −10-dB impedance bandwidth of 83% (1.58 GHz – 3.83 GHz), and a 3-dB axial ratio bandwidth of 49% (1.99 GHz – 3.27 GHz). Within the common band, the average realized gain is 6.1 dBic, and the peak realized gain is 8.6 dBic toward the front side direction of the antenna. The electrical size of the antenna is a *kr* of 1.69.

INDEX TERMS Antenna arrays, broadband antennas, microstrip antenna arrays.

I. INTRODUCTION

Microstrip antennas are a popular choice when low-profile, inexpensive, limited volume, and light weight physical design characteristics are sought after. To utilize these physical benefits, much research has been conducted to improve various electromagnetic characteristics of the microstrip patch antenna. Specifically, improving bandwidth, generating circular polarization (CP), and achieving a directive radiation pattern in a compact form have been the target.

Wideband performance allows a multitude of frequency bands to be covered by a single antenna. A rotated wide-slot antenna fed by a microstrip is a good candidate for wideband design [1]. To further increase the bandwidth, a second resonance, which combines with the original wide-slot antenna bandwidth, can be generated by a parasitic center patch [2].

CP provides greater mobility, less multipath interference, and freedom in the orientation angle between a transmitter and receiver compared to linear polarization (LP). A key metric of CP antennas is the common bandwidth (CBW) between the −10-dB impedance bandwidth (IBW) and the 3-dB axial ratio bandwidth (ARBW). The ARBW is often the limiting factor to the CBW. In [3], a circular stacked patch antenna using different truncation lengths is introduced to achieve CP. While the achieved −10-dB IBW is 64%, the CBW is 10% since the CBW is limited by the 3-dB ARBW. In [4], a patch antenna suspended above a ground plane generates a −10-dB IBW of 23%, and a comparable 3-dB ARBW, which leads to a CBW of 19%. The improved CBW is achieved through perturbation of the patch to form an H-shape, and a diagonally oriented monopole placed between the H-shaped patch and ground plane. Recently, a wideband, circularly polarized antenna with a 3-dB ARBW (64%) exceeding the −10-dB IBW (63%) is reported using a three layered structure including a L-shaped slot, feedline with matching circuit, and rotated parasitic patches located above the slot [5].

A directive radiation pattern, paired with CP, is highly pertinent to long range wireless communication systems such as mobile satellite communication, and global positioning systems. Typically, an improved realized gain can be achieved through a large antenna size, or the addition of parasitic elements. A CP microstrip patch antenna is designed by loading shorting pins between the reflector and radiating patch to increase the realized gain [6]. This method increases the realized gain to 10.3 dBic with a CBW of 1% and an electrical size, *kr* (*k* is the wave number, and *r* is the smallest radius of

The associate editor coordinating the review of this manuscript and approving it for publication was Giorgio Montisci.

an antenna encompassing sphere [7], [8]), of 5.62. A CP, half E-shaped patch antenna generates a peak realized gain greater than 7.5 dBic through the use of parasitic elements [9]. The CBW of this antenna is 9% and the electrical size, kr, is 2.01. In [10], a single layer CP antenna features a peak realized gain of 11.1 dBic through the use of a parasitic coplanar spiral strip circling a magneto-electric dipole antenna. The antenna has an electrical size, kr, of 6.85, and a CBW of 32%. Electrically small ($kr < 1$), CP, directive antennas are also reported [11], [12]. However, The CBW of these antennas are narrow since the bandwidth is bounded by a theoretical limit as the antenna size decreases [7], [8], [13].

In this paper, a novel wideband, CP, directive, two-element antenna is introduced with a truncated radiating patch fed by a microstrip line, a hexagonal wide-slot with meander tips, and a circular reflector. The hexagonal wide-slot with meander tips and near identical parasitic patch in the center of the back side of the driven element are employed to obtain a wide −10-dB IBW. The length and width of the microstrip feedline are selected to match with 50-Ω characteristic impedance effectively. Multiple truncations [14], and offset length of the microstrip feedline are primarily responsible for CP radiation. Finally, realized gain is increased by a circular reflector. All simulations are performed using CST Microwave Studio. A prototype antenna is fabricated using a LPKF milling machine. The antenna is measured in an anechoic chamber using an Agilent E5063A network analyzer.

II. PROPOSED ANTENNA

In this section the initial design hierarchy is provided to communicate the logical design steps used to reach the proposed antenna, followed by a description of the proposed antenna features, four parametric studies to determine the impact each of these parameters have on the −10-dB IBW and the 3-dB ARBW to the front side direction ($+z$) of the antenna, and an analysis of the surface current at the lower and upper bounds of the simulated CBW. Since the circular reflector's primary role is to increase the realized gain, an analysis regarding the realized gain to the front side direction ($+z$) of the antenna is included for the reflector spacing parametric study.

A. INITIAL DESIGN HIERARCHY

A theoretical analysis of the design procedure can be explained through Figure 1, the initial design hierarchy. Provided in Figure 1 is the initial structure Figure 1(a), and five subsequent iterations of minimal variance, up to the iteration before the proposed design, Figure 1(f). Each subsequent iteration includes logical changes to the antenna structure, which beneficially target specific performance characteristics. Note that a reflector is not used in Figure 1(a) - (c).

The design in Figure 1(a) is the most basic iteration, featuring a rotated slot on the back side, and an offset microstrip feedline on the front side. Figure 1(a) is designed to include 2.4 GHz initially in the −10-dB IBW. Figure 1(a) generates a LP radiation pattern. Second, a parasitic patch is added in the center of the rotated slot on the back side seen

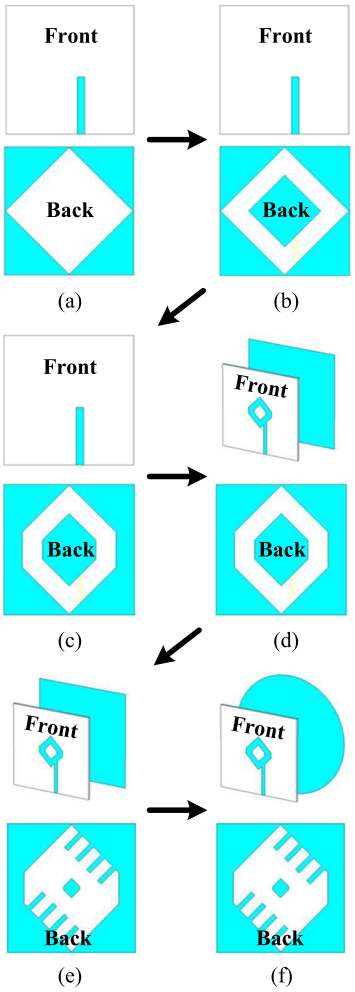

FIGURE 1. Initial antenna design hierarchy. (a) - (c) Separated front side view and back side view. (d) - (f) Separated perspective view and back side view.

in Figure 1(b). The front side of the antenna remains unchanged from Figure 1(a). Figure 1(b) is similar to the antenna found in [2]. The purpose of adding the parasitic patch in the center of the rotated slot is to improve the impedance matching of the antenna, and to provide another shorter path for current as shown by the extended −10-dB IBW in Figure 2(a) when comparing iteration "(a)" and iteration "(b)". Following Figure 1(b), Figure 1(c) incorporates the truncation of both the slot and the parasitic patch on the back side from Figure 1(b) to promote CP radiation. The front side of the antenna remains exact from Figure 1(a) and (b). At this iteration, the axial ratio (AR) is briefly reduced to below 10 dB at the lower band as shown in Figure 2(b). Next, a truncated radiating patch with the center removed is added to the top of the feedline on the front side, and a square reflector is placed in the back side direction ($-z$) as viewable in Figure 1(d). The purpose of the front side radiating patch with the center removed is to improve the −10-dB IBW and 3-dB ARBW at higher frequencies by generating an additional resonance. The AR is again altered. Seen in Figure 2(b),

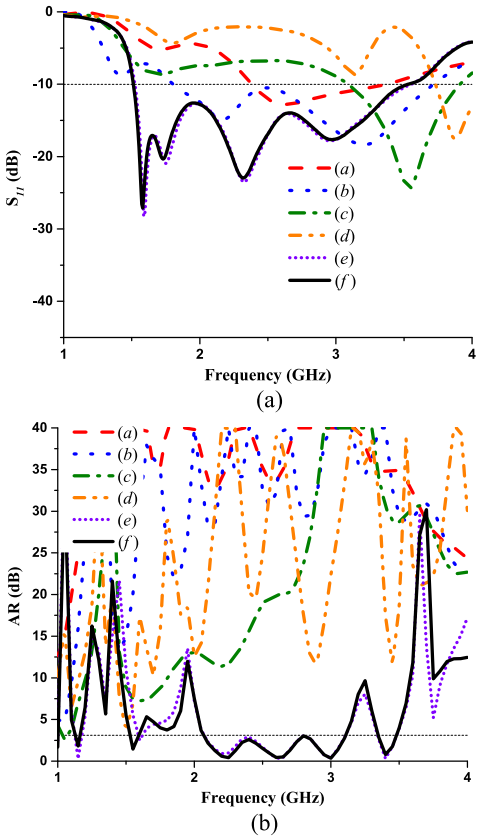

FIGURE 2. Initial antenna design hierarchy. (a) Simulated S_{11} vs. frequency. (b) Simulated AR vs. frequency.

the AR band above 2.8 GHz has dips that did not occur from iteration Figure 1(c). The directivity is improved with the addition of the reflector and forces the antenna to produce a uni-directional radiation pattern. Subsequently, the design in Figure 1(e) differs from Figure 1(d) in that Figure 1(e) features meander tips and a smaller parasitic patch. The parasitic patch is reduced in size to fit the meander tips and improve the upper band of the −10-dB IBW. Additionally, the −10-dB IBW is improved at the lower end due to the longer current path provided by the meander tips. The 3-dB ARBW becomes prevalent at this iteration, and ranges from 2.1 GHz to 3.1 GHz. Finally, in Figure 1(f) the square reflector seen in the previous iteration is replaced with a circular reflector. The primary reason for the circular reflector to make the electrical size of the antenna as small as possible. The −10-dB IBW and the 3-dB ARBW are unaffected by the change in reflector geometry.

B. ANTENNA FEATURES

The structure of the proposed wideband, CP, directive antenna is depicted in Figure 3. The proposed antenna consists of two elements; a driven microstrip patch element, and a circular reflector element. The driven element is octagonal in shape with 27 mm, *a*, and 22 mm, *b*, side lengths. The octagonal shape of the driven element is adopted to miniaturize the overall size of the antenna, as well as to increase the 3-dB ARBW.

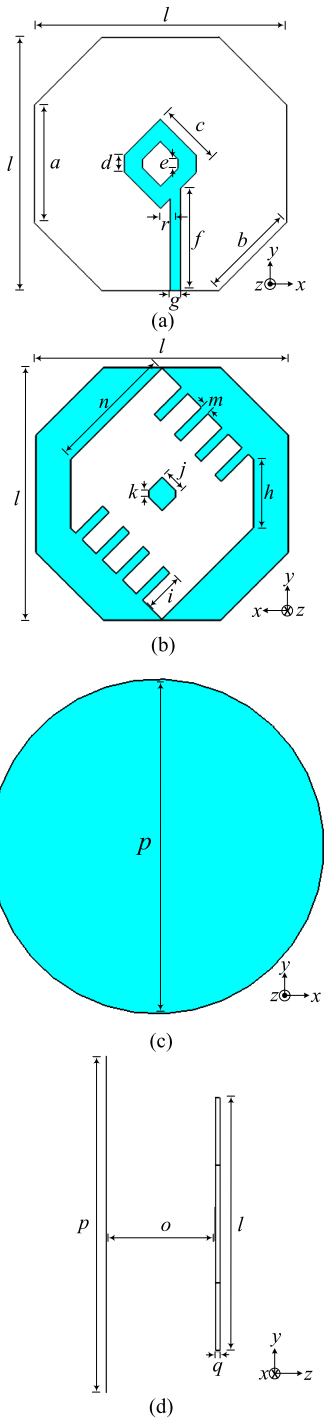

a = 27 mm (0.179λ_L)	g = 2 mm (0.013λ_L)	m = 2 mm (0.013λ_L)
b = 22 mm (0.146λ_L)	h = 16 mm (0.106λ_L)	n = 30 mm (0.200λ_L)
c = 14 mm (0.093λ_L)	i = 9 mm (0.060λ_L)	o = 39 mm (0.260λ_L)
d = 4 mm (0.027λ_L)	j = 6 mm (0.040λ_L)	p = 78 mm (0.517λ_L)
e = 2 mm (0.013λ_L)	k = 1 mm (0.006λ_L)	q = 1.6 mm (0.011λ_L)
f = 23 mm (0.153λ_L)	l = 58 mm (0.385λ_L)	r = 3 mm (0.020λ_L)

FIGURE 3. Antenna design. (a) Front side of the driven element. (b) Back side of the driven element. (c) Circular reflector. (d) Side view.

The front side of the driven element features a rotated, corner-truncated radiating patch with an inner slot of a similar shape subtracted. This subtraction is implemented to extend the current path past the microstrip feedline for wideband operation, allowing a longer current path for lower frequency resonance, and a shorter path for higher frequency resonance. The front side of the driven element also utilizes an off-center microstrip feedline. Only a single feed is utilized to keep the feeding structure simple. The feed line shift toward the $+x$ direction, r, and feed line width, g, are chosen to be 3 mm and 2 mm respectively, to maximize the -10-dB IBW and the 3-dB ARBW. The feedline offset forces the y-polarized electric field coupled from the feedline to decompose into two orthogonal components in the radiating patch. A detailed parametric studies about r and g are discussed in Section II-C.

The back side of the driven element is composed of a wide hexagonal slot inset with eight meander tips, and a parasitic patch. The eight meander tips, split evenly between two sides of the wide hexagonal slot, increase the electrical length of the sidelines, thus improving the lower band of the -10-dB IBW. The length, i, and width, m, of the meander tip are chosen to be 9 mm and 2 mm, respectively. The parasitic patch in the center of the wide hexagonal slot is the same hexagonal shape as the radiating patch on the front side, but is reduced in size. The parasitic patch is included to improve impedance matching as well as the the upper band of the 3-dB ARBW [14].

Finally, a circular reflector element is added behind the driven element to reflect the back side radiation, and consequently increase the realized gain to the front side direction ($+z$) of the antenna. The circular shape of the reflector, in comparison to a square shape reflector or large-sized frequency selective surface reflector, is used to minimize the electrical size of the proposed antenna. The distance between the circular reflector and the driven element, o, is set to 39 mm ($0.260\lambda_L$) to have a near optimal spacing for a reflector, where λ_L is calculated at 1.99 GHz, the lowest frequency of the measured CBW that will be discussed in Section III. The proposed antenna has an electrical size, kr, of 1.69 and a physical (electrical) volume of 78 mm ($0.517\lambda_L$) $\times$ 78 mm ($0.517\lambda_L$) $\times$ 40 mm ($0.265\lambda_L$). The lowest frequency in the CBW is used to calculate the electrical volume because the lowest frequency (maximum wavelength) is the dominant factor in determining the physical size of the antenna.

C. PARAMETRIC STUDY

To evaluate the effect of feed line width, g, meander tip length, i, meander tip width, m, reflector spacing, o, and feedline offset, r, parametric studies are performed. The parametric study is provided to show the effects that these presented parameters have on the -10-dB IBW and 3-dB ARBW. For a fair comparison, all parameters other than the one under test are held constant according to the values seen in Figure 3. For each study the best value, in regard to the goal, is represented by the solid black curve.

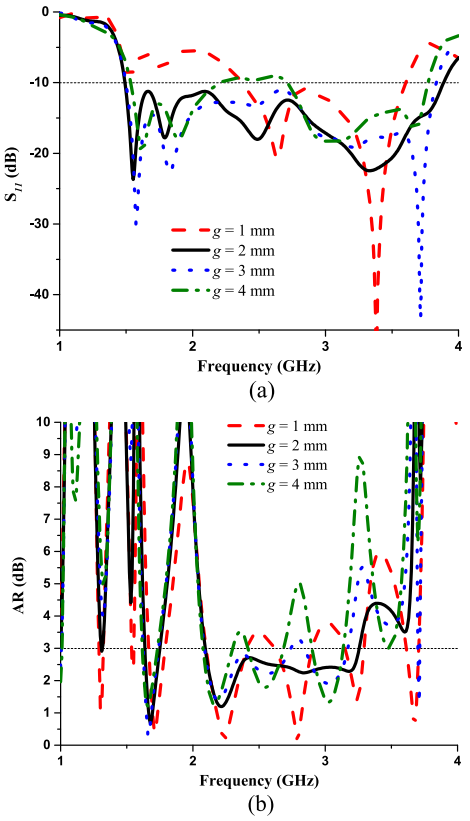

FIGURE 4. Feed width parametric study. (a) S_{11} vs. frequency. (b) AR vs. frequency.

Feed line width, g, is first tested at 1 mm, and then increased by 1 mm until 4 mm. The second value tested, 2 mm, proves to be ideal for both the -10-dB IBW and the 3-dB ARBW as seen in Figures 4(a) and (b) respectively. When g is set to 2 mm, the upper band of the -10-dB IBW is extended due to a closer matching to 50-Ω characteristic impedance. When g is set to 1 mm, the resistance is too high at both the lower and upper bands. Only when g is set to 2 mm does the ARBW remain below 3 dB for a span approaching the -10-dB IBW.

The length, i, and width, m, of the meander tips on the back side of the antenna are studied. A change in the length of the meander tips are observed, starting with 7 mm, and then incremented by 2 mm until 11 mm. The best value found for i is 9 mm. In addition to being set to 2 mm from the study performed on i, m is tested at 1 mm and 3 mm. The best value of m is 2 mm. The most notable change seen in Figures 5(a) and (b) is to the lower band of the -10-dB IBW. When the length of both i and m increases the lower -10-dB IBW becomes more prominent. Additionally, the 3-dB ARBW is only wideband for the best values of i and m.

The distance between the circular reflector and the driven element, o, is first tested at 19 mm, and then stepped up by 10 mm until 49 mm. At a reflector spacing, o, of 19 mm the lower band of the -10-dB IBW is negatively affected as seen in Figure 6(a). The negative effects at the lower band

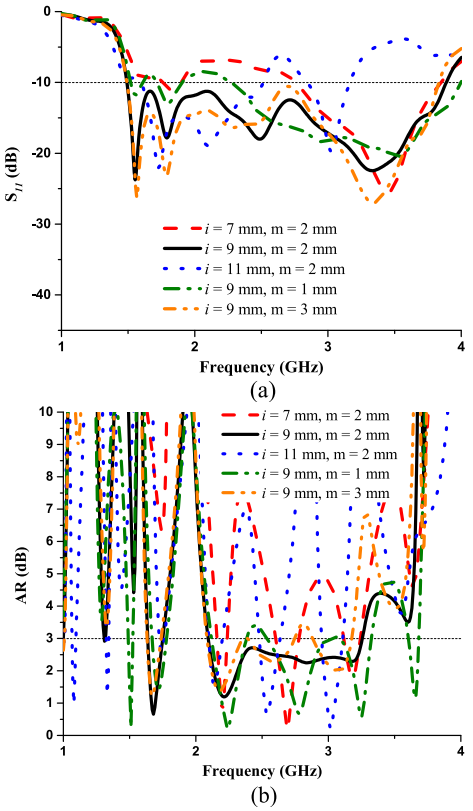

FIGURE 5. Meander tips parametric study. (a) S_{11} vs. frequency. (b) AR vs. frequency.

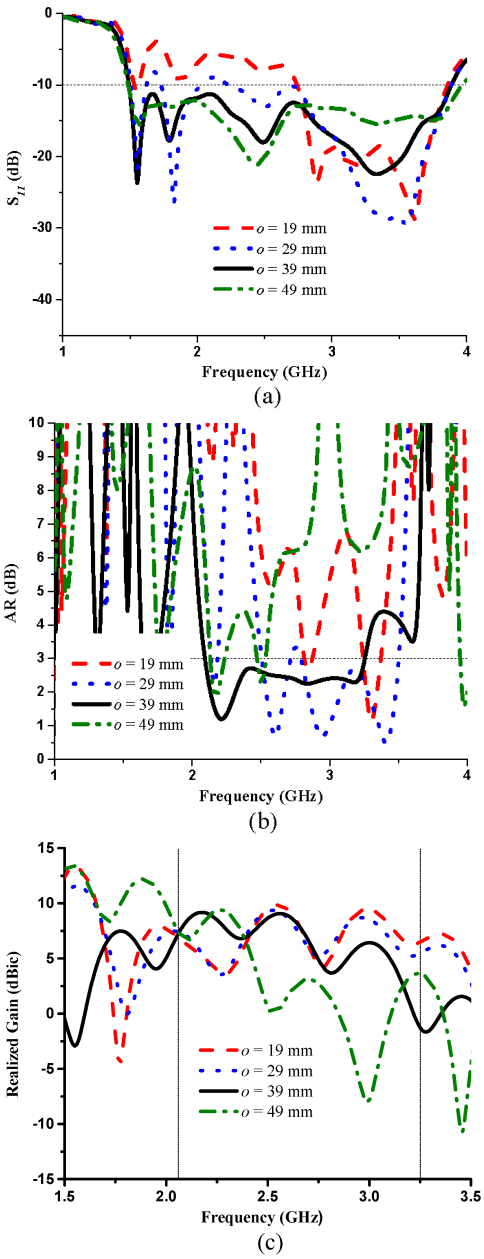

FIGURE 6. Reflector spacing parametric study. (a) S_{11} vs. frequency. (b) AR vs. frequency. (c) Realized gain vs. frequency.

occur because the closer spacing relates to quarter wavelength spacing at a higher frequency. A reflector spacing, *o*, of 29 mm creates an improvement in the lower −10-dB IBW due to the reflector being closer to a reflector spacing of quarter wavelength. The best value, 39 mm, found for spacing between the driver and parasitic reflector for the proposed antenna is similar to that of a conventional Yagi antenna, in which spacing between elements is near optimal at quarter wavelength [15]. When the reflector spacing, *o*, is set to 49 mm the −10-dB IBW is relatively unaffected compared to 39 mm, but the resonance at the upper −10-dB IBW is not as deep. Following the same pattern, closer reflector spacing resulting in higher frequency activation, the 3-dB ARBW can be explained as seen in Figure 6(b). At 19 mm, AR drops below 3 dB only at higher frequencies. Also, when the reflector spacing is 19 mm, lower frequencies such as 2.09 GHz produce a surface current on the driver that is too unbalanced with more than just the orthogonal current pairs required to generate CP radiation. At a reflector spacing, *o*, of 29 mm, the AR has additional drops at lower frequencies compared to 19 mm. For the best value for reflector spacing, 39 mm, the AR remains below 3-dB for an extended period. At a reflector spacing, *o*, of 49 mm, the AR rises above 3-dB at higher frequencies. Since the reflector's primary function is to increase the realized gain, the realized gain vs. frequency is also presented for the reflector spacing parametric study in Figure 6(c) for the four reflector spacings. The vertical lines represent the lower (2.09 GHz) and upper (3.25 GHz) bounds of the simulated CBW, which is the region of focus for the realized gain in this parameter study. A reflector spacing, *o*, of 39 mm is around a quarter wavelength of 2.09 GHz, the lowest frequency of the simulated CBW. Comparing the realized gain of the lower group (19 mm and 29 mm) to the realized gain of the proposed antenna (39 mm), it is noticeable that the realized gain is lower at lower frequencies and higher at higher frequencies. This increase of realized gain at higher frequencies of the CBW is because those lower group distances gets closer to a quarter wavelength of higher frequencies. Conversely, the realized gain of the higher group (49 mm) is noticeably higher than the realized gain of the

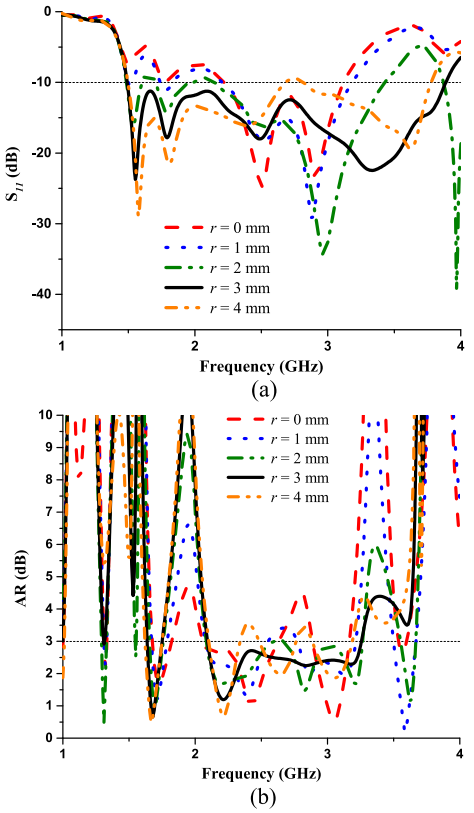

FIGURE 7. Feed position parametric study. (a) S_{11} vs. frequency. (b) AR vs. frequency.

proposed antenna (39 mm) at lower frequencies, but lower at higher frequencies of the CBW. It is because 49 mm is matched to a quarter wavelength of frequencies lower than 2.09 GHz.

Feed position, r, alters the offset of the feed in the $+x$ direction. The initial value tested, 0 mm, places the feed at the center position. The feed is then shifted by 1 mm increments until 4 mm. Both the -10-dB IBW and 3-dB ARBW are impacted by a change in r which can be seen in Figures 7(a) and (b) respectively. The best value is produced when r is set to 3 mm. When the feed position is set to the values tested below 3 mm, the lower -10-dB impedance band does not match well with 50-Ω characteristic impedance as the input resistance is too large. Additionally, the upper -10-dB impedance band does not match well for 0 mm, 1 mm, and 2 mm values of r due to increased resistance and inductance compared to 3 mm. When r is set to 4 mm it matches well at the lower band, but rises above the -10-dB threshold at around 2.7 GHz due to a more drastic increase in inductance compared to 3 mm. The 3-dB ARBW enters the lower band at the same frequency, but only when r is set to 3 mm does the ARBW remain under 3-dB for an extended period.

The side length of the parasitic patch on the back side of the antenna, j, is also tested in the order of 4 mm, 5 mm, 6 mm, 7 mm, and 8 mm. Although the best value is found to be 6 mm, adjusting j only exhibits minimal change in the upper

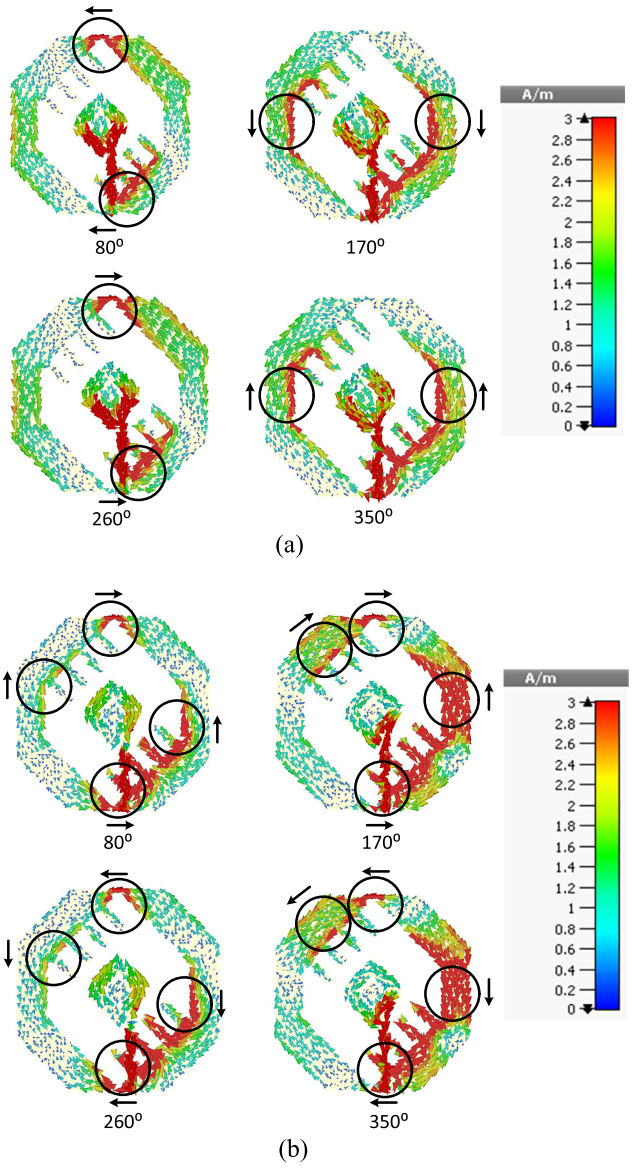

FIGURE 8. Driver surface current distribution of the front side and back side viewed from the front side direction (+z). (a) 2.09 GHz (b) 3.25 GHz.

band of the -10-dB IBW and the 3-dB ARBW. Therefore, the effect that j has on the -10-dB IBW and 3-dB ARBW is not sensitive with changes of up to ± 2 mm.

D. SURFACE CURRENT

The surface current distributions of the front side and the back side of the proposed antenna viewed from the front side ($+z$) at the lowest and highest bounds of the simulated CBW, 2.09 GHz and 3.25 GHz, are displayed in Figure 8. The phase at each frequency is shifted by 90° increments starting at 80° to best demonstrate the properties of the proposed antenna. The substrate is hidden so that both the current on the front side of the antenna, the radiating patch and shifted feedline, and the back side of the antenna can be seen from the front side ($+z$) view. The strongest areas of current on the back side of the proposed antenna are circled for importance, and

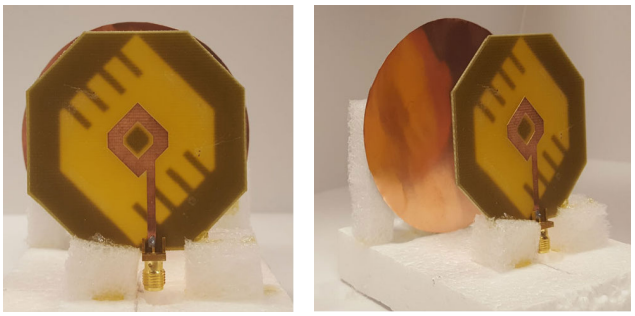

(a) (b)

FIGURE 9. Fabricated antenna. (a) Front view. (b) Slanted view.

the direction of current is emphasized by the arrows. The reflector is not shown in the current study due to negligible current strength. The surface current on the reflector at both 2.09 GHz and 3.25 GHz are less than 0.5 (A/m).

At 2.09 GHz the proposed antenna shows strong current on both the inside and outside of the back side of the antenna seen in Figure 8(a). At 2.09 GHz, the back side features two clear concentrations of strong current. Surface current captured at a 90° phase shift, for example 80° and 170°, demonstrate orthogonal current patterns which are required for CP radiation. The feed is located at the bottom of the feedline, therefore the current is stronger near the bottom of the antenna. The surface current on the front side extends a path length relative to frequency. The lower the frequency, the further the current path travels along the feedline and radiating patch.

When observed at the highest bound of the simulated CBW, 3.25 GHz, the proposed antenna generates strong current concentrations in four areas on the back side of the antenna seen in Figure 8(b). At 3.25 GHz the strong current flowing on the left and right side of the proposed antenna are not entirely symmetrical for all phases. This current imbalance results in a slanted radiation pattern at higher frequencies.

III. SIMULATION AND EXPERIMENTAL RESULTS

The copper features on the driven element are milled from the top and bottom layers of a commercially available, double-sided FR4 substrate with a permittivity of 4.4 and a loss tangent of 0.02. The thickness of the FR4 substrate is 1.6 mm. A Pyralux copper sheet is cut to create the reflector. The fabricated antenna is shown in Figure 9.

Figure 10 shows the simulated and measured S_{11} curve of the antenna. The simulated −10-dB IBW is 89% (1.49 GHz – 3.88 GHz), and the measured −10-dB IBW is 83% (1.58 GHz – 3.83 GHz). The 3-dB ARBW in the front side direction ($+z$) of the antenna is depicted in Figure 11. In simulation, the antenna has a 3-dB ARBW of 44% (2.09 GHz – 3.25 GHz), and in measurement the antenna has a 3-dB ARBW of 49% (1.99 GHz – 3.27 GHz). Measurement results for both the −10-dB IBW and the 3-dB ARBW show good agreement with simulated ones. The CBW is calculated from the smallest overlapped band between −10-dB IBW and 3-dB ARBW. For the proposed antenna, the CBW is equivalent to

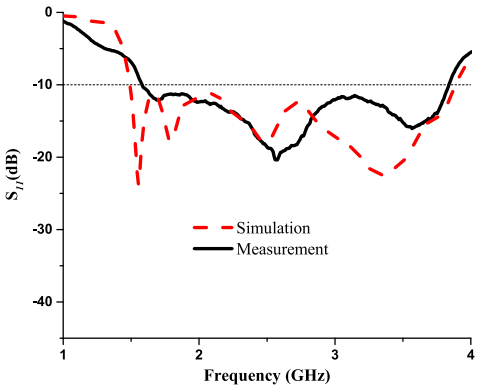

FIGURE 10. Simulated and measured S_{11} vs. frequency.

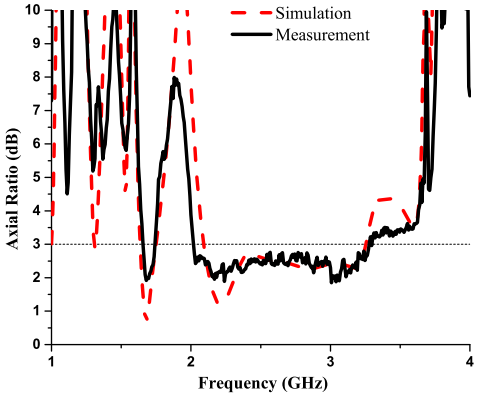

FIGURE 11. Simulated and measured AR vs. frequency.

the 3-dB ARBW because the 3-dB ARBW is fully within the −10-dB IBW range for both simulation and measurement. The proposed antenna, which is compact and directive, can cover numerous applications and can be used for multi-purpose. The measured CBW of the proposed antenna (1.99 GHz – 3.27 GHz) covers applications including mobile satellite communications working at 2 GHz and 2.2 GHz, 2.1 GHz UMTS, 2.4 GHz WLAN, 2.3 GHz and 2.5 GHz WiMAX, and 3 GHz marine navigation systems.

Simulated and measured realized gain patterns are presented in Figure 12 at the 25th (2.38 GHz), 50th (2.67 GHz) and 75th (2.96 GHz) percentile of the simulated CBW. Measured results agree well with simulated ones at all three frequencies in both the xz plane and yz plane. The 3-dB beamwidth of the antenna is observed to be greater than 67° for both the xz plane and yz plane at all frequencies. The antenna is directive toward $+z$ direction, and the front-to-back ratio is more than 5 dB in both simulation and measurement. As agrees with the surface current analysis in Section II-D, the radiation patterns tilt as frequency increases due to unbalanced current. While the radiation is titled, the realized gain toward the $+z$ direction is still over 5 dBic. Note that the sense of the proposed antenna is right handed (RH) towards the front side direction ($+z$) of the antenna. Since the radiation pattern of the antenna is directive toward the front side direction ($+z$) of the antenna, the back

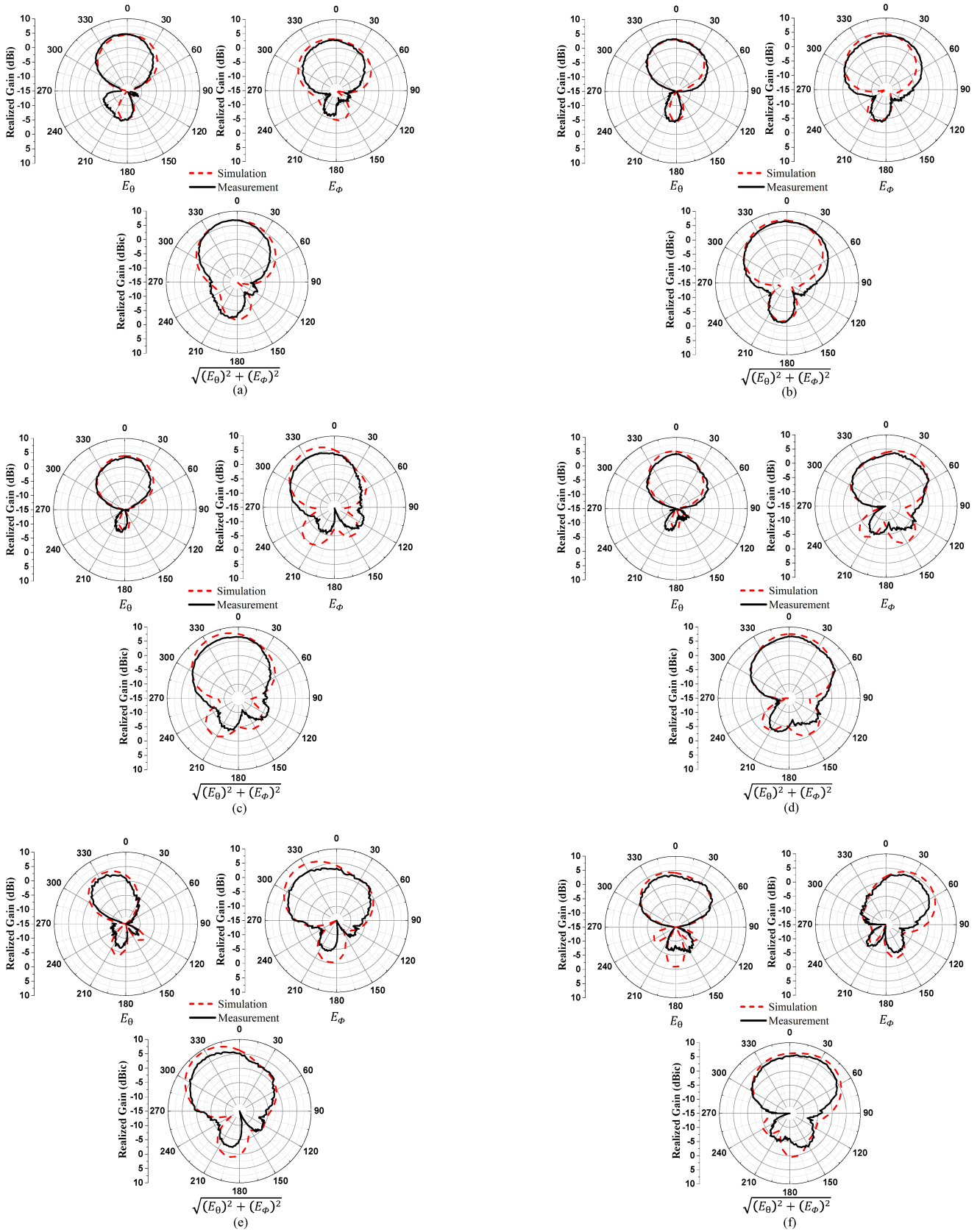

FIGURE 12. Realized gain patterns. At 2.38 GHz in, (a) *xz* plane. (b) *yz* plane. At 2.67 GHz in, (c) *xz* plane. (d) *yz* plane. At 2.96 GHz in, (e) *xz* plane. (f) *yz* plane.

TABLE 1. Comparison of circularly polarized antennas.

	Frequency, f_L (GHz)	Overall Volume (λ_L^3)	Electrical Size (kr)	-10-dB IBW (GHz)	3-dB ARBW (GHz)	CBW (GHz)	Peak Realized Gain (dBic)	Figure of Merit
[3]	5.70	NA	NA	3.30 -6.40 (64%)	5.70-6.30 (10%)	5.70-6.30 (10%)	6.4	NA
[4]	2.28	$1.67\lambda_L \times 1.67\lambda_L \times 0.24\lambda_L$	7.4	2.21-2.77 (23%)	2.28-2.77 (19%)	2.28-2.77 (19%)	5.7	0.15
[5]	2.20	$0.29\lambda_L \times 0.68\lambda_L \times 0.03\lambda_L$	2.32	2.20-4.20 (63%)	2.10-4.20 (64%)	2.20-4.20 (63%)	1.8	0.49
[6]	2.53	$0.51\lambda_L \times 0.51\lambda_L \times 0.03\lambda_L$	5.62	2.50-2.64 (5%)	2.53-2.56 (1%)	2.53-2.56 (1%)	10.3	0.02
[9]	0.85	$0.43\lambda_L \times 0.43\lambda_L \times 0.07\lambda_L$	2.01	0.83-0.96 (14%)	0.85-0.93 (9%)	0.85-0.93 (9%)	7.5	0.34
[10]	13.20	$1.54\lambda_L \times 1.54\lambda_L \times 0.13\lambda_L$	6.85	11.40-18.50 (52%)	13.20-18.00 (32%)	13.20-18.00 (32%)	11.1	0.52
[11]	0.43	$0.17\lambda_L \times 0.17\lambda_L \times 0.02\lambda_L$	0.74	0.43-0.43 (1%)	0.43-0.43 (1%)	0.43-0.43 (1%)	3.5	0.05
[12]	0.15	$0.26\lambda_L \times 0.26\lambda_L \times 0.03\lambda_L$	0.84	0.15-0.15 (1%)	0.14-0.15 (1%)	0.15-0.15 (1%)	5.4	0.06
[16]	2.38	$0.23\lambda_L \times 0.23\lambda_L \times 0.01\lambda_L$	1.55	2.25-4.00 (56%)	2.38-4.60 (64%)	2.38-4.00 (51%)	3.5	1.15
[17]	2.20	$0.54\lambda_L \times 0.45\lambda_L \times 0.01\lambda_L$	2.22	2.20-3.70 (51%)	2.00-3.40 (47%)	2.20-3.40 (43%)	NA	NA
[18]	1.69	$0.28\lambda_L \times 0.28\lambda_L \times 0.01\lambda_L$	1.25	1.68-3.20 (62%)	1.69-2.92 (53%)	1.69-2.92 (53%)	4.2	1.78
[19]	1.50	$0.74\lambda_L \times 0.36\lambda_L \times 0.01\lambda_L$	2.53	0.80-4.15 (136%)	1.50-3.40 (77%)	1.50-3.40 (77%)	4.1	1.25
[20]	2.13	$0.38\lambda_L \times 0.27\lambda_L \times 0.01\lambda_L$	1.47	1.99-4.28 (73%)	2.13-3.43 (47%)	2.13-3.43 (47%)	2.6	0.83
[21]	2.18	$0.65\lambda_L \times 0.65\lambda_L \times 0.12\lambda_L$	2.92	2.18-2.81 (25%)	2.18-2.73 (22%)	2.18-2.73 (22%)	8.2	0.62
[22]	1.06	$0.27\lambda_L \times 0.27\lambda_L \times 0.07\lambda_L$	1.19	0.96-1.20 (22%)	1.06-1.14 (7%)	1.06-1.14 (7%)	5.4	0.32
[23]	2.18	$0.59\lambda_L \times 0.59\lambda_L \times 0.19\lambda_L$	2.70	2.18-3.92 (57%)	2.15-3.50 (48%)	2.18-3.50 (46%)	7.5*	1.28
This Work	1.99	$0.39\lambda_L \times 0.39\lambda_L \times 0.27\lambda_L$	1.69	1.58-3.83 (83%)	1.99-3.27 (49%)	1.99-3.27 (49%)	8.6	2.49

Note: All values are from measurement results unless otherwise stated. Electrical size is calculated from the lowest frequency (f_L) in the CBW. Peak realized gain is limited to the CBW range. *Simulation results (measurement result not provided).

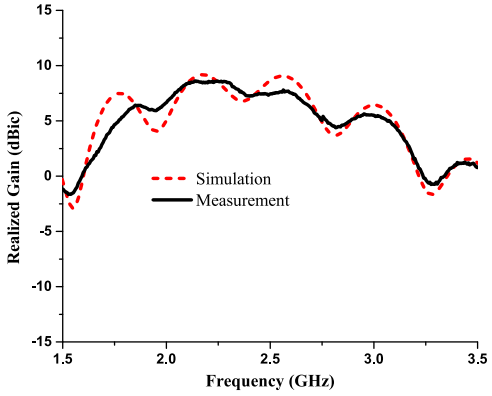

FIGURE 13. Simulated and measured realized gain toward the front side direction (+z) of the antenna vs. frequency.

side ($-z$) LHCP radiation is negligible (less than 0 dBic in simulation).

Figure 13 shows the simulated and measured realized gain vs. frequency toward the front side direction ($+z$) of the antenna. In simulation, the average realized gain is 6.4 dBic in the simulated CBW (2.09 – 3.25 GHz), with a peak realized gain of 9.2 dBic at 2.18 GHz. The measurement results in an average realized gain of more than 6.1 dBic in the CBW (1.99 GHz – 3.27 GHz), and a peak realized gain of 8.6 dBic at 2.20 GHz. The agreement between simulation and measurement is good.

Table 1 provides a comprehensive comparison of measurement results between the proposed antenna and previously reported work relating to CP antennas. This comparison includes the lowest frequency of the CBW, overall volume, electrical size, −10-dB IBW, 3-dB ARBW, CBW, peak realized gain, and Figure of Merit. As seen in Table 1, the −10-dB IBW is wider than the 3-dB ARBW in the majority of CP antennas. Using the data found in Table 1, the rightmost column of Table 1 features a Figure of Merit metric for fair comparison. The Figure of Merit is calculated by the following equation

$$\frac{(\text{CBW})(\text{Peak Realized Gain})}{\text{Electrical Size, } kr} \tag{1}$$

A higher Figure of Merit indicates an antenna with a better combination of CBW, peak realized gain, and electrical size (kr). Note that the proposed antenna has the highest Figure of Merit of 2.49. The second highest Figure of Merit in the comparison table is found with [18] at a value of 1.78. The average Figure of Merit for the antennas found in Table 1, not including the proposed antenna, is 0.63. For additional comparison, the Figure of Merit of a conventional CP corner truncated patch antenna is 0.03 with a maximum CBW of 2% [14], peak realized gain of 2.3 dBic, and electrical size of 1.7.

IV. CONCLUSION

A two-element antenna is introduced to increase the CBW between the −10-dB IBW and 3-dB ARBW, to enhance the realized gain, and to minimize the electrical size simultaneously. In the driven element, the front side radiating patch, back side hexagonal slot with meander tips, and parasitic patch of similar shape in the center of the back side of the driven element are designed to generate multiple resonances.

A circular-shaped reflector is added to increase the realized gain. The proposed antenna exhibits a measured CBW of 49% with a frequency range of 1.99 GHz to 3.27 GHz (−10-dB IBW of 83% with a frequency range of 1.58 GHz to 3.83 GHz and 3-dB ARBW of 49% with a frequency range of 1.99 GHz to 3.27 GHz). Also in measurement, the proposed antenna produces an average realized gain of about 6.1 dBic in the CBW and peak realized gain of 8.6 dBic toward the front side direction ($+z$) of the antenna. The electrical size of the antenna, kr, is 1.69. With a compact size, the proposed wideband, directive, CP antenna has promising potential for future generation wireless communication systems with multi-functional capability.

REFERENCES

[1] J.-Y. Jan and J.-W. Su, "Bandwidth enhancement of a printed wide-slot antenna with a rotated slot," *IEEE Trans. Antennas Propag.*, vol. 53, no. 6, pp. 2111–2114, Jun. 2005.
[2] Y. Sung, "Bandwidth enhancement of a microstrip line-fed printed wide-slot antenna with a parasitic center patch," *IEEE Trans. Antennas Propag.*, vol. 60, no. 4, pp. 1712–1716, Apr. 2012.
[3] Y.-X. Guo and D. C. H. Tan, "Wideband single-feed circularly polarized patch antenna with conical radiation pattern," *IEEE Antennas Wireless Propag. Lett.*, vol. 8, pp. 924–926, 2009.
[4] K. L. Chung, "A wideband circularly polarized H-shaped patch antenna," *IEEE Trans. Antennas Propag.*, vol. 58, no. 10, pp. 3379–3383, Oct. 2010.
[5] R. Pazoki, A. Kiaee, P. Naseri, H. Moghadas, H. Oraizi, and P. Mousavi, "Circularly polarized monopole L-shaped slot antenna with enhanced axial-ratio bandwidth," *IEEE Antennas Wireless Propag. Lett.*, vol. 15, pp. 1073–1076, 2016.
[6] X. Zhang and L. Zhu, "High-gain circularly polarized microstrip patch antenna with loading of shorting pins," *IEEE Trans. Antennas Propag.*, vol. 64, no. 6, pp. 2172–2178, Jun. 2016.
[7] L. J. Chu, "Physical limitations of omni-directional antennas," *J. Appl. Phys.*, vol. 19, no. 12, pp. 1163–1175, 1948.
[8] D. F. Sievenpiper, D. C. Dawson, M. M. Jacob, T. Kanar, S. Kim, J. Long, and R. G. Quarfoth, "Experimental validation of performance limits and design guidelines for small antennas," *IEEE Trans. Antennas Propag.*, vol. 60, no. 1, pp. 8–19, Jan. 2012.
[9] J. Li, H. Liu, S. Zhang, M. Luo, Y. Zhang, and S. He, "A wideband single-fed, circularly-polarized patch antenna with enhanced axial ratio bandwidth for UHF RFID reader applications," *IEEE Access*, vol. 6, pp. 55883–55892, 2018.
[10] W. Cao, Q. Wang, Z. Qian, S. Shi, J. Jin, K. Ding, and B. Zhang, "Gain enhancement for wideband CP ME-dipole antenna by loading with spiral strip in Ku-band," *IEEE Trans. Antennas Propag.*, vol. 66, no. 2, pp. 962–966, Feb. 2018.
[11] J. J. Yu and S. Lim, "Design of an electrically small, circularly polarized, parasitic array antenna for an active 433.92-MHz RFID handheld reader," *IEEE Trans. Antennas Propag.*, vol. 60, no. 5, pp. 2549–2554, May 2012.
[12] S. Lim, J. Chen, and C. Cato, "Design of a thin, electrically small, two-element parasitic array with circular polarization," *IEEE Antennas Wireless Propag. Lett.*, vol. 17, pp. 1006–1009, 2018.
[13] H. A. Wheeler, "Fundamental limitations of small antennas," *Proc. IRE*, vol. 35, pp. 1479–1484, Dec. 1947.
[14] S. Gao, Q. Luo, and F. Zhu, *Circularly Polarized Antennas*. Hoboken, NJ, USA: Wiley, 2014.
[15] W. L. Stutzman and G. A. Thiele, *Antenna Theory Design*, 3rd ed. Hoboken, NJ, USA: Wiley, 2013.
[16] M. Samsuzzaman, M. T. IsLam, and M. J. Singh, "A compact printed monopole antenna with wideband circular polarization," *IEEE Access*, vol. 6, pp. 54713–54725, 2018.
[17] O. Ahmad Mashaal, S. K. A. Rahim, A. Y. Abdulrahman, M. I. Sabran, M. S. A. Rani, and P. S. Hall, "A coplanar waveguide fed two arm archimedean spiral slot antenna with improved bandwidth," *IEEE Trans. Antennas Propag.*, vol. 61, no. 2, pp. 939–943, Feb. 2013.
[18] H. Bagheroghli, "A novel circularly polarized microstrip antenna with two connected quasi monopoles for wideband applications," *IEEE Antennas Wireless Propag. Lett.*, vol. 12, pp. 1343–1346, 2013.
[19] K. G. Thomas and P. G, "A novel wideband circularly polarized printed antenna," *IEEE Trans. Antennas Propag.*, vol. 60, no. 12, pp. 5564–5570, Dec. 2012.
[20] Y.-M. Cai, K. Li, Y.-Z. Yin, and W. Hu, "Broadband circularly polarized printed antenna with branched microstrip feed," *IEEE Antennas Wireless Propag. Lett.*, vol. 13, pp. 674–677, 2014.
[21] X. H. Tang, Y. L. Long, H. Wong, and K. L. Lau, "Broadband circularly-polarised patch antenna with 3D meandering strip feed," *Electron. Lett.*, vol. 47, no. 19, pp. 1060–1062, Sep. 2011.
[22] X. Chen, L. Yang, J.-Y. Zhao, and G. Fu, "High-efficiency compact circularly polarized microstrip antenna with wide beamwidth for airborne communication," *IEEE Antennas Wireless Propag. Lett.*, vol. 15, pp. 1518–1521, 2016.
[23] S. L. S. Yang, A. A. Kishk, and K. F. Lee, "Wideband circularly polarized antenna with L-shaped slot," *IEEE Trans. Antennas Propag.*, vol. 56, no. 6, pp. 1780–1783, Jun. 2008.

TYLER J. MCPHERSON (S'19) was born in New Brunswick, NJ, USA, in 1994. He received the B.S. degree in electrical and computer engineering from Georgia Southern University, Statesboro, GA, USA, in 2018, where he is currently pursuing the M.S. degree in electrical engineering.

Since 2018, he has been a Graduate Assistant with the Electrical and Computer Engineering Department, Georgia Southern University, Statesboro. His research interests include antennas, specifically directive antennas, electrically small antennas, and printable antennas.

ZABED IQBAL (S'16) was born in Dhaka, Bangladesh, in 1991. He received the B.Sc. degree in electrical, electronic, and communication engineering from the Military Institute of Science and Technology, Dhaka, in 2012, and the M.S. degree in electrical engineering from Georgia Southern University, Statesboro, GA, USA, in 2017. He is currently pursuing the Ph.D. degree in electrical engineering with The University of Alabama in Huntsville, Huntsville, AL, USA.

From 2013 to 2015, he was a Lecturer and a Coordinator with the Department of Electrical and Electronic Engineering, Z. H. Sikder University of Science and Technology, Bangladesh. His research interests include antennas, phased array radars, and electromagnetics.

SUNGKYUN LIM (S'03–M'07–SM'14) was born in Seoul, South Korea, in 1975. He received the B.S. degrees in electrical and computer engineering and mathematics from Hanyang University, Seoul, in 1999, and the M.S. and Ph.D. degrees in electrical and computer engineering from The University of Texas at Austin, Austin, TX, USA, in 2004 and 2007, respectively.

He was a Research Assistant and a Teaching Assistant with The University of Texas at Austin, Austin. From 2007 to 2011, he was an Assistant Professor with the Hawaii Center for Advanced Communications, College of Engineering, University of Hawai'i at Mānoa, Honolulu, HI, USA. From 2011 to 2015, he was an Assistant Professor with the Department of Computer Engineering, Georgia Southern University, Statesboro, GA, USA. Since 2015, he has been an Associate Professor and the Graduate Program Director with the Department of Computer Engineering, Georgia Southern University, Statesboro. He has authored over 80 journal articles and conference proceedings. His research interests are in the area of analysis and design of antennas in wireless communications, including electrically small antennas, supergain arrays, RFID, wireless power transfer, optimization methods, metamaterials, and propagation modeling.

Dr. Lim was a recipient of the Georgia Research for Academic Partnership in Engineering (GRAPE) Award and the Georgia Southern Faculty Development Award.